How to cite: *Angew. Chem. Int. Ed.* **2023**, *62*, e202308089
doi.org/10.1002/anie.202308089

Asymmetric Catalysis | Hot Paper

Turning on Asymmetric Catalysis of Achiral Metal-Organic Frameworks by Imparting Chiral Microenvironment

Ge Yang[+], Wenwen Shi[+], Yunyang Qian, Xiao Zheng, Zheng Meng, and Hai-Long Jiang**

Abstract: The development of heterogeneous asymmetric catalysts has attracted increasing interest in synthetic chemistry but mostly relies on the immobilization of homogeneous chiral catalysts. Herein, a series of chiral metal–organic frameworks (MOFs) have been fabricated by anchoring similar chiral hydroxylated molecules (catalytically inactive) with different lengths onto Zr-oxo clusters in achiral PCN-222(Cu). The resulting chiral MOFs exhibit regulated enantioselectivity up to 83 % *ee* in the asymmetric ring-opening of cyclohexene oxide. The chiral molecules furnished onto the catalytic Lewis sites in the MOF create multilevel microenvironment, including the hydrogen interaction between the substrate and the chiral –OH group, the steric hindrance endowed by the benzene ring on the chiral molecules, and the proximity between the catalytic sites and chiral molecules confined in the MOF pores, which play crucial roles and synergistically promote chiral catalysis. This work nicely achieves heterogeneous enantioselective catalysis by chiral microenvironment modulation around Lewis acid sites.

Introduction

Chirality, widely existing in the fields of medicine, chemical industry, agriculture, etc., is crucial for life and science. Pharmaceutical research has proven that enantiomers with inverted chirality have dramatically different biological activities. Therefore, it is of great importance and interest to develop simple and efficient strategies to synthesize optically pure compounds.[1] Over the past few decades, privileged homogeneous chiral catalysts have been developed, such as salen complexes, bis(oxazoline) ligands, and cinchona alkaloid derivatives.[2] However, the synthesis of these chiral ligands is usually too elaborate with complicated asymmetric reactions,[3] and the non-recyclability of homogeneous catalysts poses additional challenges for their practical use. Hence, heterogeneous chiral catalysts have emerged as alternatives to homogeneous chiral catalysts. The immobilization of homogeneous chiral catalysts onto supports is a generally accepted strategy, for which, unfortunately, the leaching of active components is commonly observed during the reaction.[4]

To meet this challenge, a creative solution has been developed to heterogenize homogeneous chiral catalysts by assembling them into crystalline porous skeletons, i.e., metal–organic frameworks (MOFs). As a class of porous crystalline solids, MOFs feature well-defined and tailorable structures, high surface area and uniform high-density active sites,[5] being intensively investigated in heterogeneous catalysis.[6] Diverse homogeneous chiral catalysts, serving as functional organic subunits, have been periodically assembled with metal-oxo clusters into chiral MOFs, addressing the above issue of active component leaching and well demonstrating the great advantages and potential toward chiral catalysis.[7] Despite significant success in many cases, careful exploration of the reaction recipes for the time- and labor-consuming synthesis of chiral ligands and MOFs is necessary. There have been very few reports on the construction of chiral MOFs by simple post-synthetic modification, and they are essentially related to the heterogenization of homogeneous chiral catalysts.[8] In fact, the post-synthetic modification of MOFs provides opportunities to create chiral microenvironment around the common active sites in the confined MOF pore space, thereby achieving chiral catalysis, which offers us a conceptually different way to create heterogeneous chiral MOFs.

As thus, the construction of enzyme-mimicking chiral MOFs by post-synthetic chiral modification would be possible. Generally, the catalytic pockets of enzymes are responsible for the excellent activity and selectivity,[9] which are derived from the precise and unique arrangement of amino acid residues. The catalytic sites in enzymes are responsible for binding to specific substrates, and their activation and conversion.[9b,c] The local physicochemical microenvironment cooperates with catalytic site to rectify the reaction kinetics and substrate selectivity. The microenvironment surrounding catalytic site promotes the interaction between binding groups and substrate and maintains

[*] G. Yang,[+] Dr. Y. Qian, Prof. Dr. Z. Meng, Prof. Dr. H.-L. Jiang
Hefei National Research Center for Physical Sciences at the Microscale, Department of Chemistry, University of Science and Technology of China
230026 Hefei, Anhui (P. R. China)
E-mail: jianglab@ustc.edu.cn
Homepage: http://mof.ustc.edu.cn/
W. Shi,[+] Prof. Dr. X. Zheng
CAS Key Laboratory of Precision and Intelligent Chemistry, University of Science and Technology of China
230026 Hefei, Anhui (P. R. China)
E-mail: xz58@ustc.edu.cn
Prof. Dr. X. Zheng
Department of Chemistry, Fudan University
200433 Shanghai (P. R. China)
[+] These authors contributed equally to this work.

the conformation of enzyme, leading to the final catalytic performance.[10] Inspired by that in enzyme catalysis, multiple-level chiral microenvironment in the MOF pore space, alike enzyme pocket-like, to some extent, can be fabricated.[11] In this case, the challenging synthesis of homogeneous chiral metal complexes is no longer necessary, and direct adoption of common symmetric MOFs for chiral catalysis becomes possible by creating specific chiral microenvironment around the existing catalytic sites via elaborate post-synthetic modification.

To verify the above assumption, in this work, a centrosymmetric PCN-222(Cu) in *P6/mmm* space group was adopted as a representative to construct chiral catalysts. A series of chiral molecules of (*R*)–C_n–COOH with similar structures but different lengths of carbon chains, including (*R*)-2-hydroxy-2-phenylacetic acid, (*R*)-2-hydroxy-3-phenylpropionic acid, and (*R*)-2-hydroxy-4-phenylbutanoic acid, respectively, termed as (*R*)–C_1–COOH, (*R*)–C_2–COOH, and (*R*)–C_3–COOH, are grafted onto the unsaturated coordination sites of Zr-oxo cluster in PCN-222(Cu) (Scheme 1). The resulting chiral catalysts exhibit excellent catalytic performance in the asymmetric ring-opening of cyclohexene oxide, where (*R*)–C_3@PCN-222(Cu) affords the best enantioselectivity (up to 83 % *ee*), followed by (*R*)–C_1@PCN-222(Cu) (67 % *ee*) and (*R*)–C_2@PCN-222(Cu) (35 % *ee*). The exposed Zr-oxo cluster in the MOF works as Lewis acid sites to drive the reaction, and the multilevel microenvironment modulation around the Zr-oxo cluster plays critical roles in the resulting enantioselectivity: 1) The dangling chiral –OH group of (*R*)–C_n–COOH interacts with substrates via weak hydrogen bonding, serving as the chiral induction; 2) The presence of benzene ring on the flexible carbon chains in different lengths gives rise to steric hindrance, greatly affecting the chiral induction level; 3) The confined mesopore in PCN-222(Cu), behaving as the nanoreactor of chiral catalysis, further improves the enantioselectivity. Control experiments illustrate that the *ee* values can be significantly improved only when the chiral and catalytic sites are confined in MOFs and in close proximity to each other. To the best of our knowledge, this is the first report on achieving chiral catalysis in MOFs by microenvironment modulation surrounding catalytic sites.

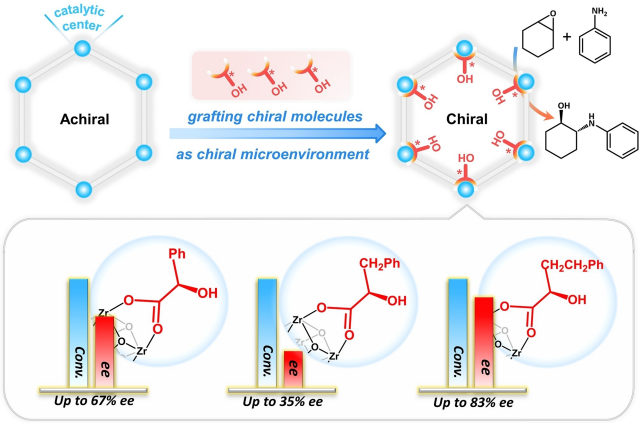

Scheme 1. Schematic illustration showing (top) the synthetic protocol of (*R*)–C_n@PCN-222(Cu) and (bottom) their catalytic results in the asymmetric ring-opening of cyclohexene oxide.

Results and Discussion

The highly stable Zr-based MOF, PCN-222(Cu), consisting of $Zr_6(\mu_3\text{–}O)_4(\mu_3\text{–}OH)_4(OH)_4(H_2O)_4(COO)_8$ clusters and Cu-centered tetrakis(4-carboxyphenyl)-porphyrin (TCPP) linkers, was synthesized according to the previous report.[12] Solvent-assisted ligand incorporation (SALI) approach was adopted to graft enantiomerically pure C_n–COOH onto Zr-oxo clusters of PCN-222(Cu) to afford chiral C_n@PCN-222(Cu) (Figure S1).[13a] The C_n–COOH enantiomers in *R* and *S* configurations have been confirmed by circular dichroism (CD) spectra (Figure S2), and their chirality has been well inherited to the resulting PCN-222(Cu) (Figure 1).

Diffuse reflectance infrared Fourier transform spectroscopy (DRIFTS) measurements provide the coordination information of Zr-oxo clusters, in which the peak of the terminal –OH at 3671 cm^{-1} disappears while the shoulder at 3663 cm^{-1} assigned to bridging μ_3–OH groups still exists after the SALI process, suggesting that the terminal –OH groups were replaced by chiral (*R*)–C_n–COOH molecules (Figure 2a).[13] The degree of post-synthetic modification onto Zr-oxo clusters has been quantitatively analyzed by ^1H nuclear magnetic resonance (NMR) (Figure 2b). The integrated area of ^1H signal of C_n–COOH reveals that an average of 3.8–3.9 chiral molecules are grafted onto each Zr-oxo cluster, indicating almost complete replacement of the dangling –OH groups (Figure S3). Compared with pristine PCN-222(Cu), nitrogen sorption isotherms indicate that the BET surface area of (*R*)–C_n@PCN-222(Cu) reasonably decreases due to the pore space occupation by the grafted carbon chains (Figure 2c), supporting the retained highly

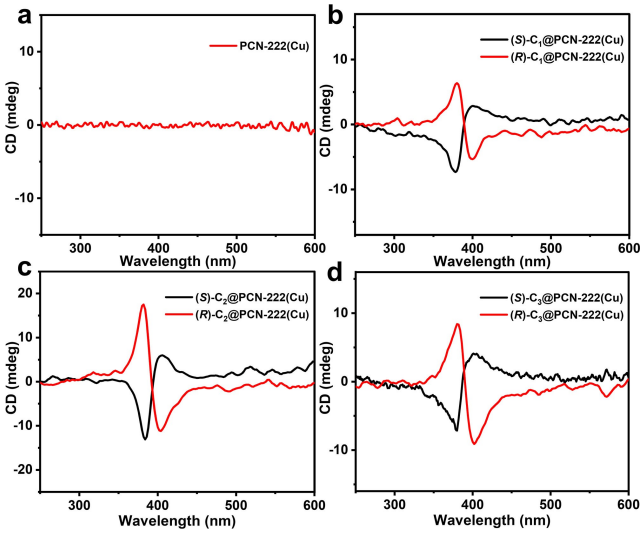

Figure 1. CD spectra of (a) pristine PCN-222(Cu), and the enantiomers of (b) C_1@PCN-222(Cu), (c) C_2@PCN-222(Cu), and (d) C_3@PCN-222(Cu).

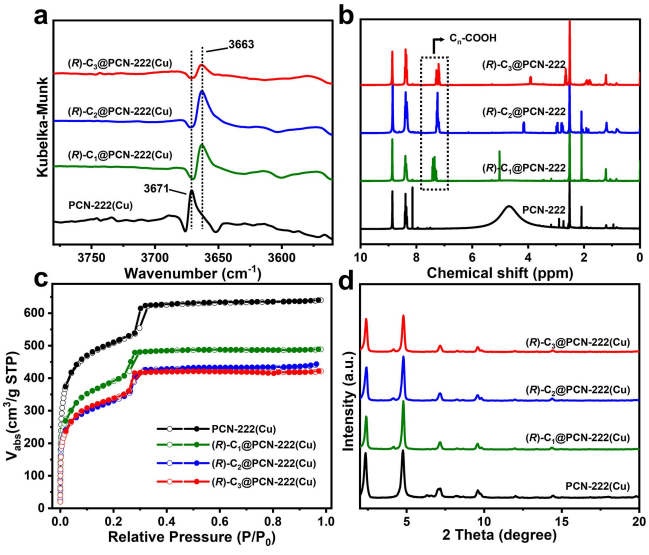

Figure 2. (a) DRIFT spectra, (b) ^{1}H NMR spectra, (c) N_2 sorption isotherms at 77 K, and (d) powder XRD patterns of PCN-222(Cu) and (*R*)–C_n@PCN-222(Cu) ($n=1, 2, 3$).

porous feature after the modification (Figure S4). Scanning electron microscopy (SEM) images reveal that the rod-shaped morphology of PCN-222(Cu) does not change after the post-modification (Figure S5). Powder X-ray diffraction (XRD) patterns demonstrate that the crystallinity of the MOF is well maintained after grafting the chiral modifiers (Figure 2d), manifesting its stability. Thermogravimetric analysis (TGA) and differential thermal analysis (DTA) curves present three weight loss steps, in which an exothermic temperature range at 200–300 °C possibly resulting from the loss of C_n–COOH is observed (Figure S6), further supporting the successful introduction of the chiral modifiers.

Given the catalytic sites confined in PCN-222(Cu) channels with furnished chiral microenvironment, serving as enzyme-like binding pockets, we assume that the obtained catalysts would be promising candidates in challenging and important enantioselective reactions. Asymmetric ring-opening of racemic epoxides by amines is an important platform in organic synthesis to prepare amino alcohols with two chiral centers. They are not only valuable components in the synthesis of many natural drugs, but also can be used as chiral catalysts or ligands for asymmetric catalytic reactions.[14a] With this in mind, asymmetric ring-opening of cyclohexene oxide with aniline has been adopted to investigate their catalytic performance.[14] To our delight, the results show that all (*R*)–C_n@PCN-222(Cu) exhibit excellent conversion to the target product of 2-(phenylamino) cyclohexanol in the reaction of cyclohexene oxide and aniline (Figure S7, S8), unambiguously demonstrating their high activities toward ring-opening of epoxides. Strikingly, the highest enantioselectivity obtained by (*R*)–C_3@PCN-222(Cu) reflects the more efficient chiral induction by using (*R*)–C_3–COOH than (*R*)–C_1–COOH and (*R*)–C_2–COOH (Figure S9).

Based on the above results, the optimal reaction conditions for the asymmetric ring-opening of cyclohexene oxide with aniline over (*R*)–C_3@PCN-222(Cu) have been screened by changing the solvents, temperature, and catalyst loading (Table S1). When the asymmetric ring-opening cyclohexene oxide is operated in toluene at 25 °C in the presence of 10 mol % catalyst of (*R*)–C_3@PCN-222(Cu), an optimal yield of >99 % with an 83 % *ee* can be achieved in 10 hours. Under the identical conditions, (*R*)–C_2@PCN-222(Cu) and (*R*)–C_1@PCN-222(Cu) afford >99 % yield with *ee* values of 35 % and 67 %, respectively (Table 1, entries 1–3), supporting the role of chiral (*R*)–C_n–COOH anchored onto PCN-222(Cu) in modulating the chiral selectivity (*ee*). Moreover, the scope of substrates has also been evaluated by using (*R*)–C_3@PCN-222(Cu) under the optimal conditions (Table S2). The electronic properties and position of the substituents present significant influence on the yield and *ee* value of the corresponding products. It is assumed that, some racemic products might be generated due to the limited "unmodified" Zr sites with the chiral modifiers, which accounts for the <100 % *ee* values of the resulting products.

To probe the specific structural factors of modified chiral (*R*)–C_n–COOH contributed to the enantioselectivity, control experiments have been conducted (Figure S10, S11). When the hydroxyl group of (*R*)–C_1–COOH is replaced by the methyl group, only racemic products are obtained (Figure S12a), which is probably due to that the chiral modifier without hydroxyl group fails to direct the attack position of aniline through hydrogen bonds. This result suggests the indispensable function of the hydroxyl group in generating enantioselectivity. In fact, the presence of hydrogen interaction between aniline and the –OH group of the chiral modifier can be supported by the concentration-dependent peak shift in the ^{1}H NMR spectra for aniline with

Table 1: Asymmetric ring-opening reaction of cyclohexene oxide with aniline catalyzed by different catalysts.[a]

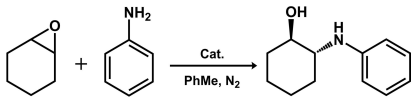

Entry	Catalyst	Yield[b] [%]	*ee*[c] [%]
1	(*R*)–C_1@PCN-222(Cu)	>99	67
2	(*R*)–C_2@PCN-222(Cu)	>99	35
3	(*R*)–C_3@PCN-222(Cu)	>99	83
4	(*R*)–C_3–COOH	14	3
5	TCPP(Cu)-ester	trace	–
6	Zr-oxo cluster	88	−1
7	PCN-222(Cu)	97	−1
8	(*R*)–C_3/PCN-222(Cu)	>99	60
9	(*R*)–C_3-ester/PCN-222(Cu)	93	0
10	(*R*)–$Zr_6(OH)_4O_4(C_3–COO)_{12}$	89	10
11	(*R*)–C_3/Zr_6 cluster	91	−4

[a] Reaction conditions: catalyst (10 mol %), aniline (0.1 mmol), cyclohexene oxide (0.12 mmol), 1 mL toluene, N_2 atmosphere, $T=25$ °C, time = 10 hours. [b] Yield of product was obtained by GC with n-dodecane as the internal standard. [c] Enantioselectivity of product was analyzed by HPLC with AD–H chiral column.

the ester form of (*R*)–C_3–COOH (Figure S11b). Furthermore, when the benzene ring of (*R*)–C_1–COOH is substituted by different groups, including isobutyl, methyl, and isopropyl, the enantiomeric excess values display significant decrease with decreased sizes of the substituents (Figure S12b–d). Despite that the enantioselectivity is chiral modifier dependent, the nonlinear relationship between the enantioselectivity and the size of the substituent may be a sign that the enantioselectivity is not contributed solely by the steric effect from the chiral modifier, but determined by the overall chiral microenvironment. The above results emphasize the decisive relationship between the hydrogen-bonding interaction created by the hydroxyl group of the chiral modifier and the resulting enantioselectivity; meanwhile, the size (steric hindrance) of the chiral modifiers is also responsible for the chiral selectivity, possibly with the cooperation of other structural factors in the MOF catalysts.

The catalytic performance of the homogeneous chiral molecules, the main component in PCN-222(Cu) and their physical mixture have been assessed to demonstrate the superiority of chiral (*R*)–C_n@PCN-222(Cu) architectures (Table 1). The use of (*R*)–C_3–COOH gives a poor yield of 14% and negligible enantioselectivity (Table 1, entry 4), indicating that (*R*)–C_3–COOH has a very limited catalytic capability for the reaction, despite that the acidity of carboxylic acid may promote the formation of the product, and that (*R*)–C_n–COOH alone is not able to generate chiral induction effect (Figure S13). Particularly, the undetectable yield acquired by TCPP(Cu)-ester excludes the possibility of the central Cu(II) in the porphyrin center as the catalytic site (Table 1, entry 5), hinting that the catalytic centers are possibly stemmed from coordinatively unsaturated Zr-oxo clusters. In comparison to (*R*)–C_3–COOH, the use of the Zr-oxo clusters and PCN-222(Cu) as catalysts can afford the yield of 88% and 97%, respectively; however, racemic products are obtained (Table 1, entries 6 and 7). The much higher yields provided by Zr-oxo clusters and PCN-222(Cu) than that by (*R*)–C_3–COOH reinforce the dominant catalytic role of Zr-oxo clusters in (*R*)–C_n@PCN-222(Cu) toward the ring-opening of cyclohexene oxide. This is likely because the strong Lewis acidity of Zr-oxo clusters can activate cyclohexene oxide to facilitate the subsequent amino nucleophilic attack.[15]

The physical mixture of PCN-222(Cu) and (*R*)–C_3–COOH exhibits 60% *ee* value after complete conversion (Table 1, entry 8). The enantioselectivity is much smaller than that of (*R*)–C_3@PCN-222(Cu) with 83% *ee* (Table 1, entry 3), indicating the importance of immobilizing chiral modifiers onto the MOF skeleton. In fact, we assume that, the mixture of (*R*)–C_3–COOH and PCN-222(Cu) will spontaneously interact during the catalytic reaction to in situ generate (*R*)–C_n@PCN-222(Cu) to a certain degree, the latter of which plays a critical role in the final enantioselectivity. To prove this point, (*R*)–C_3-ester, in which the carboxylic group of (*R*)–C_3–COOH is blocked to avoid its coordination to Zr-oxo clusters, is adopted to prepare the physical mixture, (*R*)–C_3-easter/PCN-222(Cu). As expected, the negligible enantioselectivity by the (*R*)–C_3-easter/PCN-222(Cu) further demonstrates the necessity of immobilizing chiral modifiers onto the MOF (Table 1, entry 9). Given these findings, it is inferred that the close proximity between the chiral molecules and catalytic sites is of great importance in the catalytic process, during which the space confinement effect created by the MOF pore space should play a key role in achieving high enantioselectivity. To verify the above hypothesis, the Zr-oxo cluster has been synthesized, followed by grafting (*R*)–C_3–COOH, to afford (*R*) –$Zr_6(OH)_4O_4(C_3–COO)_{12}$ (Figure S14), in which the space confinement effect is absent. The *ee* values obtained from (*R*) –$Zr_6(OH)_4O_4(C_3–COO)_{12}$ and the mixture of (*R*)–C_3–COOH and Zr-oxo clusters are both significantly lower than that of (*R*)–C_3@PCN-222(Cu) (Table 1, entries 10 and 11). The results unambiguously suggest that, not only the close proximity between the chiral molecules and catalytic sites, but also the space confinement effect endowed by PCN-222(Cu) are indispensable to the high enantioselectivity of (*R*)–C_3@PCN-222(Cu).

The heterogeneous nature and recyclability of (*R*)–C_3@PCN-222(Cu) have been evaluated. The similar kinetic curves detected by (*R*)–C_n@PCN-222(Cu) ($n=1$, 2, 3) reflect their similar catalytic capability (Figure S15). When the catalyst is filtered out after 90 min of reaction, no more product is formed (Figure S15c), indicating the catalyst is truly heterogeneous. The catalyst can be recovered by centrifugation and reused for at least five runs without appreciable loss of activity or enantioselectivity (Figure S16), demonstrating its high durability. Powder XRD patterns reveal the crystallinity is well maintained after the reaction (Figure S17), further verifying the excellent stability of chiral (*R*)–C_n@PCN-222(Cu). The DRIFT spectra of (*R*)–C_n@PCN-222(Cu) after catalytic reaction have been collected and the terminal –OH at 3671 cm^{-1} is not observed (Figure S18), reflecting that the chiral modifiers don't leach from the Zr-oxo cluster. To examine whether the reaction occurs inside the MOF, tetradecanoic acid, a long chain alkene with molecular size of 20.76 Å × 5.42 Å × 4.02 Å, is adopted as a modifier to decorate onto the unsaturated Zr-oxo clusters for blocking the pores of PCN-222(Cu). The resulting tetradecanoic acid@PCN-222(Cu) displays a much inferior kinetic curve compared to (*R*)–C_n@PCN-222(Cu) in the ring-opening reaction of cyclohexene oxide with aniline (Figure S15, S19), providing direct evidence for the catalytic reaction occurring inside the MOF.

To gain insights into the mechanism and understand the enantioselectivity difference in the asymmetric ring-opening reaction catalyzed by (*R*)–C_n@PCN-222(Cu), density functional theory (DFT) calculations have been employed.[16] Given the large number of atoms in (*R*)–C_n@PCN-222(Cu), a reasonable simplification is made for the structural units posing negligible influence on the reaction environment (Figure S20, Table S3–S5). The bond lengths and atomic charges of cyclohexene oxide exhibit negligible changes upon coordination with Zr atom, and no radical species are generated during the process, indicating that it would belong to an SN2 mechanism rather than SN1 mechanism (Figure S21). This suggests that the Lewis acid activation and the nucleophilic attack occur simultaneously. According to the calculated mechanism diagram (Figure S22, S23), the

cyclohexene oxide is firstly accessible to the Zr-oxo cluster by competing coordination with (*R*)–C_n–COOH, which leads to the disconnection of one O atom of the carboxylic acid with the Zr atom of the Zr-oxo cluster. At the same time, hydrogen bonds are formed between –NH_2 of aniline and –OH of the chiral modifier, placing aniline in a preferred position (Figure S24, structure A). Subsequently, the N atom of –NH_2 group attacks the C atom of cyclohexene oxide when aniline approaches to epoxy ring (Figure S24, structures B, TS and C), and then 2-(phenylamino) cyclohexanol is generated along with H shift from NH_2 to the ring-open O atom (Figure S24, structure D). Finally, desorption occurs, and the (*R*)–C_n–COOH and Zr-oxo clusters recover their initial coordination state (Figure S24, structure E). Notably, the transition state in asymmetric ring-opening reaction exhibits a ring-like structure, which is collectively formed by the chiral molecules, Zr-oxo clusters and reactants, proving that the close proximity between chiral sites and catalytic sites is favorable to the formation of the transition state structure (Figure S25).

The calculated Gibbs free energy difference (ΔG, indicated by black arrows) for the transition state of (*R*, *R*)-product is smaller than that of the (*S*, *S*)-product (Figure 3), suggesting that the product with *R* configuration is more favorable than that with *S* configuration in the catalytic process. Furthermore, the differences of ΔG for the formation of product with *S* and *R* configuration mediated by (*R*)–C_1@PCN-222(Cu) and (*R*)–C_2@PCN-222(Cu) are computed to be 4.30 and 2.03 kcal mol^{-1}, respectively (Figure 3b, c), both of which are smaller than that of (*R*)–C_3@PCN-222(Cu) (6.89 kcal mol^{-1}, Figure 3d). These computational results support the enantioselectivity trend of (*R*)–C_n@PCN-222(Cu) experimentally determined, which is in the order of (*R*)–C_3@PCN-222(Cu) > (*R*)–C_1@PCN-222(Cu) > (*R*)–C_2@PCN-222(Cu) (Table 1). The ΔG induced by (*R*)-2-hydroxy-3-methylbutanoic acid@PCN-222(Cu) is also calculated, where the benzene ring of (*R*)–C_1–COOH is substituted with isopropyl. As expected, its ΔG differences is smaller than (*R*)–C_1@PCN-222(Cu), computationally supporting the steric effect from benzene ring of chiral modifier (Figure S26). A closer inspection of the optimized transition state structures indicates that the enantioselectivity may be closely related to the distance between the nucleophilic N atom and the attacked C atom (Figure S27). For (*R*)–C_3@PCN-222(Cu) with the highest selectivity, the difference of N···C lengths in the two transition states for the (*R, R*)- and (*S, S*)-products is the most significant. On the contrary, the N···C lengths in the two transition states are very close for (*R*)–C_2@PCN-222(Cu), leading to the lowest enantioselectivity. The vertical and parallel alignment between the plane of benzene ring and carboxyl group of chiral molecules ((*R*)–C_n–COOH) is determined by the odevity of n, where the structural difference may be responsible for the nonlinear trend of the enantioselectivity of (*R*)–C_n@PCN-222(Cu).

To unveil the weak interactions in catalytic system, the independent gradient model based on Hirshfeld partition (IGMH) analysis has been carried out (Figure 4 and S28–S30).[17] Remarkably, the area of the red isosurface at the center of the transition state (between the O atom and N atom) represents the steric hindrance of the weak interaction, which can be qualitatively measured by the sign(λ_2)ρ corresponding to the maximum δg in the red region. The (*R*, *R*)-product catalyzed by (*R*)–C_3@PCN-222(Cu) exhibits a minimum value of sign(λ_2)ρ, indicating that the transition state experiences minimal steric hindrance (Figure 4). When computing the sign(λ_2)ρ difference among *R* or *S* configuration products obtained by the same chiral catalyst, the following trend is observed: (*R*)–C_3@PCN-222(Cu)

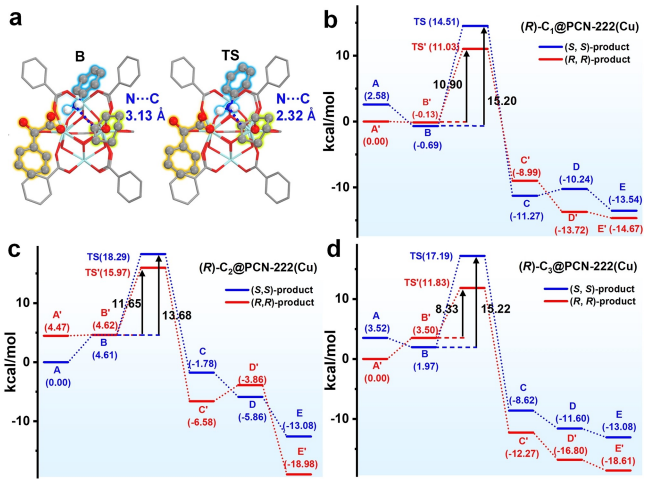

Figure 3. (a) Optimized structures of B and TS (transition state) of ring-opening reaction for (*R*)–C_1@PCN-222(Cu). The hydrogen atoms are omitted for clarity except on –NH_2 (C, gray; H, white; O, red; N, blue and Zr, bluish green). The free energy profiles along the pathway for the asymmetric ring-opening of epoxides over (b) (*R*)–C_1@PCN-222(Cu), (c) (*R*)–C_2@PCN-222(Cu), and (d) (*R*)–C_3@PCN-222(Cu), respectively. The Gibbs free energy of the more stable structure A/A′ is set to zero energy.

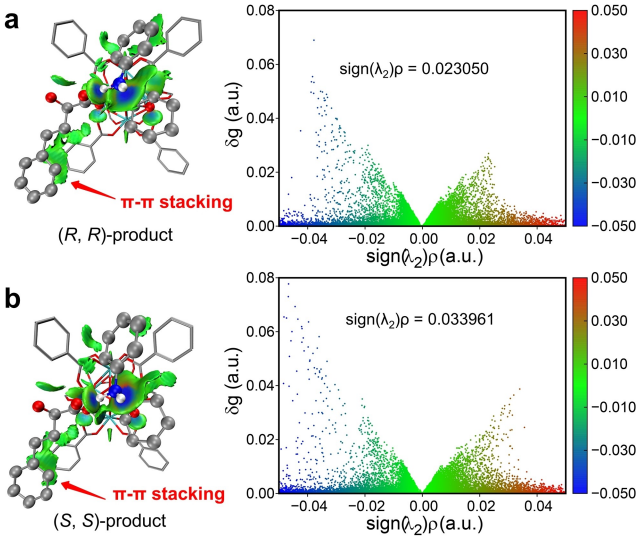

Figure 4. Sign(λ_2)ϱ colored isosurfaces of $\delta g^{inter} = 0.005$ a.u. corresponding to IGMH analysis of (a) (*R*, *R*)-product and (b) (*S*, *S*)-product with catalyst (*R*)–C_3@PCN-222(Cu).

(0.0109) > (*R*)–C_1@PCN-222(Cu) (0.0084) > (*R*)–C_2@PCN-222(Cu) (0.0035) > no catalyst (0.0021), which is closely associated with the experimental trend. When n is an odd number in (*R*)–C_n@PCN-222(Cu), the benzene ring plane of (*R*)–C_n–COOH is perpendicular to the carboxylic acid group plane. During the formation of the transition state, the perpendicular benzene ring closely interacts with the ligand benzene ring of PCN-222(Cu), resulting in robust π–π stacking interactions (Figure 4 and S29). This π–π stacking interaction plays a significant role in promoting and facilitating the formation of the transition state, which accounts for the observed non-monotonic selectivity order in (*R*)–C_n@PCN-222(Cu) as follows: (*R*)–C_3@PCN-222(Cu) -> (*R*)–C_1@PCN-222(Cu) > (*R*)–C_2@PCN-222(Cu).

Conclusion

In summary, the centrosymmetric MOF, PCN-222(Cu) in *P6/mmm* space group, has been converted to the chiral MOFs, affording (*R*)–C_n@PCN-222(Cu), by a simple post-synthetic modification with chiral molecules (*R*)–C_n–COOH ($n = 1, 2, 3$) onto the Zr-oxo cluster in the MOF. The resulting heterogeneous (*R*)–C_n@PCN-222(Cu) catalysts are able to not only achieve chiral catalysis but also regulate the enantioselectivity in the asymmetric ring-opening of cyclohexene oxide, in which the modification with chiral molecules creates multi-level microenvironment modulation around the catalytic sites, i.e. Zr-oxo cluster. Control experiments demonstrate that the hydroxyl groups from the chiral modifier, capable of forming hydrogen bonds with substrate along the MOF channel, play a decisive role in ensuring enantioselective catalysis. Not only the close proximity between the chiral molecules and catalytic sites but also the space confinement effect endowed by the MOF are also proven to be indispensable to achieve high enantioselectivity. All these microenvironment modulations lead to non-linearly evolved enantioselectivity with the change of chiral modifier in (*R*)–C_n@PCN-222(Cu), among which the *ee* value follows the order of (*R*)–C_3@PCN-222(Cu) > (*R*)–C_1@PCN-222(Cu) > (*R*)–C_2@PCN-222(Cu). This trend is further validated and explained by DFT calculations. This work not only opens a door to the synthesis of chiral MOFs by post-synthetic modification with chiral molecules, but also provides a novel strategy to the design of heterogeneous chiral catalysts by simply creating specific chiral microenvironment around catalytic sites.

Acknowledgements

This work is supported by the National Key Research and Development Program of China (2021YFA1500402), the Strategic Priority Research Program of the Chinese Academy of Sciences (XDB0450302), the National Natural Science Foundation of China (U22A20401, 22161142001), and International Partnership Program of CAS (123GJHZ2022028MI).

Conflict of Interest

The authors declare no conflict of interest.

Data Availability Statement

The data that support the findings of this study are available from the corresponding author upon reasonable request.

Keywords: Asymmetric Catalysis · Heterogeneous Catalysis · Metal-Organic Frameworks · Microporous Materials

[1] a) T. Akiyama, I. Ojima, in *Catalytic Asymmetric Synthesis*, Wiley-VCH, Weinheim, **2022**.
[2] a) T. P. Yoon, E. N. Jacobsen, *Science* **2003**, *299*, 1691–1693; b) D. W. C. MacMillan, *Nature* **2008**, *455*, 304–308; c) S. Shaw, J. D. White, *Chem. Rev.* **2019**, *119*, 9381–9426; d) G. Yang, W. Zhang, *Chem. Soc. Rev.* **2018**, *47*, 1783–1810; e) C. Portolani, G. Centonze, P. Righi, G. Bencivenni, *Acc. Chem. Res.* **2022**, *55*, 3551–3571.
[3] a) D. Zhang, Z. Su, Q. He, Z. Wu, Y. Zhou, C. Pan, X. Liu, X. Feng, *J. Am. Chem. Soc.* **2020**, *142*, 15975–15985; b) D. A. Kutateladze, C. C. Wagen, E. N. Jacobsen, *J. Am. Chem. Soc.* **2022**, *144*, 15812–15824; c) L. Zhang, Z. Wang, Z. Han, K. Ding, *Angew. Chem. Int. Ed.* **2020**, *59*, 15565–15569.
[4] a) M. B. Buendia, S. Kegnæs, S. Kramer, *Adv. Synth. Catal.* **2020**, *362*, 5506–5512; b) Y. Saito, S. Kobayashi, *J. Am. Chem. Soc.* **2020**, *142*, 16546–16551; c) Y. Saito, S. Kobayashi, *Angew. Chem. Int. Ed.* **2021**, *60*, 26566–26570.
[5] a) H. Furukawa, K. E. Cordova, M. O'Keeffe, O. M. Yaghi, *Science* **2013**, *341*, 1230444; b) R.-B. Lin, Z. Zhang, B. Chen, *Acc. Chem. Res.* **2021**, *54*, 3362–3376; c) S. Horike, S. Kitagawa, *Nat. Mater.* **2022**, *21*, 983–985; d) A. N. Hong, H. Yang, X. Bu, P. Feng, *EnergyChem* **2022**, *4*, 100080; e) K.-Y. Wang, Z. Yang, J. Zhang, S. Banerjee, E. A. Joseph, Y.-C. Hsu, S. Yuan, L. Feng, H.-C. Zhou, *Nat. Protoc.* **2023**, *18*, 604–625; f) Y.-S. Wei, L. Zou, H.-F. Wang, Y. Wang, Q. Xu, *Adv. Energy Mater.* **2022**, *12*, 2003970; g) M.-S. Yao, W.-H. Li, G. Xu, *Coord. Chem. Rev.* **2021**, *426*, 213479.
[6] a) G. Li, S. Zhao, Y. Zhang, Z. Tang, *Adv. Mater.* **2018**, *30*, 1800702; b) J. Liu, T. A. Goetjen, Q. Wang, J. G. Knapp, M. C. Wasson, Y. Yang, Z. H. Syed, M. Delferro, J. M. Notestein, O. K. Farha, J. T. Hupp, *Chem. Soc. Rev.* **2022**, *51*, 1045–1097; c) L. Zeng, X. Guo, C. He, C. Duan, *ACS Catal.* **2016**, *6*, 7935–7947; d) Y.-B. Huang, J. Liang, X.-S. Wang, R. Cao, *Chem. Soc. Rev.* **2017**, *46*, 126–157; e) S. Navalón, A. Dhakshinamoorthy, M. Álvaro, B. Ferrer, H. García, *Chem. Rev.* **2023**, *123*, 445–490; f) L. Jiao, J. Wang, H.-L. Jiang, *Acc. Mater. Res.* **2021**, *2*, 327–339; g) Y.-L. Yang, Y.-R. Wang, L.-Z. Dong, Q. Li, L. Zhang, J. Zhou, S.-N. Sun, H.-M. Ding, Y. Chen, S.-L. Li, Y.-Q. Lan, *Adv. Mater.* **2022**, *34*, 2206706; h) C. Feng, Z.-P. Wu, K.-W. Huang, J. Ye, H. Zhang, *Adv. Mater.* **2022**, *34*, 2200180; i) L. Li, Z. Li, W. Yang, Y. Huang, G. Huang, Q. Guan, Y. Dong, J. Lu, S.-H. Yu, H.-L. Jiang, *Chem* **2021**, *7*, 686–698; j) L. Jiao, H.-L. Jiang, *Chin. J. Catal.* **2023**, *45*, 1–5.
[7] a) Z. Xia, C. He, X. Wang, C. Duan, *Nat. Commun.* **2017**, *8*, 361; b) W. Gong, X. Chen, W. Zhang, K. O. Kirlikovali, B. Nan, Z. Chen, R. Si, Y. Liu, O. K. Farha, Y. Cui, *J. Am. Chem. Soc.* **2022**, *144*, 3117–3126; c) M. Pan, K. Wu, J.-H. Zhang, C.-Y. Su, *Coord. Chem. Rev.* **2019**, *378*, 333–349; d) C. Kutzscher, H. C. Hoffmann, S. Krause, U. Stoeck, I. Senkovska, E. Brunner, S. Kaskel, *Inorg. Chem.* **2015**, *54*, 1003–1009; e) L. Ma, J. M. Falkowski, C. Abney, W. Lin, *Nat. Chem.* **2010**, *2*,

838–846; f) N. Antil, N. Akhtar, R. Newar, W. Begum, A. Kumar, M. Chauhan, K Manna, *ACS Catal.* **2021**, *11*, 10450–10459; g) T.-Y. Zhou, B. Auer, S. J. Lee, S. G. Telfer, *J. Am. Chem. Soc.* **2019**, *141*, 1577–1582; h) Y. Zhang, S. Chen, A.-M. Al-Enizi, A. Nafady, Z. Tang, S. Ma, *Angew. Chem. Int. Ed.* **2022**, *62*, e202213399; i) R. E. Morris, X. Bu, *Nat. Chem.* **2010**, *2*, 353–361.

[8] a) K. D. Nguyen, C. Kutzscher, F. Drache, I. Senkovska, S Kaskel, *Inorg. Chem.* **2018**, *57*, 1483–1489; b) M. Banerjee, S. Das, M. Yoon, H. J. Choi, M. H. Hyun, S. M. Park, G. Geo, K. Kim, *J. Am. Chem. Soc.* **2009**, *131*, 7524–7525.

[9] a) S. J. Benkovic, S. Hammes-Schiffer, *Science* **2003**, *301*, 1196–1202; b) Y.-P. Xue, C.-H. Cao, Y.-G. Zheng, *Chem. Soc. Rev.* **2018**, *47*, 1516–1561; c) J. Wu, X. Guan, Z. Dai, R. He, X. Ding, L. Yang, G. Ge, *Coord. Chem. Rev.* **2021**, *427*, 213600.

[10] a) Q. Fu, X. Bao, *Nat. Catal.* **2019**, *2*, 834–836; b) J. C. Fontecilla-Camps, A. Volbeda, *Chem. Rev.* **2022**, *122*, 12110–12131; c) J. Wang, C. D. Buchman, J. Seetharaman, D. J. Miller, A. D. Huber, J. Wu, S. C. Chai, E. Garcia-Maldonado, W. C. Wright, J. Chenge, T. Chen, *J. Am. Chem. Soc.* **2021**, *143*, 18467–18480; d) J. P. López-Alonso, M. Lázaro, D. Gil-Cartón, P. H. Choi, L. Tong, M. Valle, *Nat. Commun.* **2022**, *13*, 6185.

[11] a) B. Hou, S. Yang, K. Yang, X. Han, X. Tang, Y. Liu, J. Jiang, Y. Cui, *Angew. Chem. Int. Ed.* **2021**, *60*, 6086–6093; b) H.-C. Ma, C.-C. Zhao, G.-J. Chen, Y.-B. Dong, *Nat. Commun.* **2019**, *10*, 3368; c) J. Jiao, J. Dong, Y. Li, Y. Cui, *Angew. Chem. Int. Ed.* **2021**, *60*, 16568–16575.

[12] a) D. Feng, Z.-Y. Gu, J.-R. Li, H.-L. Jiang, Z. Wei, H.-C. Zhou, *Angew. Chem. Int. Ed.* **2012**, *51*, 10307–10310; b) W. Morris, B. Volosskiy, S. Demir, F. Gandara, P. L. McGrier, H. Furukawa, D. Cascio, J. F. Stoddart, O. M. Yaghi, *Inorg. Chem.* **2012**, *51*, 6443–6445; c) Y. Chen, T. Hoang, S. Ma, *Inorg. Chem.* **2012**, *51*, 12600–12602.

[13] a) P. Deria, J. E. Mondloch, E. Tylianakis, P. Ghosh, W. Bury, R. Q. Snurr, J. T. Hupp, O. K. Farha, *J. Am. Chem. Soc.* **2013**, *135*, 16801–16804; b) X. Ma, H. Liu, W. Yang, G. Mao, L. Zheng, H.-L. Jiang, *J. Am. Chem. Soc.* **2021**, *143*, 12220–12229.

[14] a) C. Wang, L. Luo, H. Yamamoto, *Acc. Chem. Res.* **2016**, *49*, 193–204; b) H. Bao, J. Wu, H. Li, Z. Wang, T. You, K. Ding, *Eur. J. Org. Chem.* **2010**, 6722–6726; c) N. Deshpande, A. Parulkar, R. Joshi, B. Diep, A. Kulkarni, N. A. Brunelli, *J. Catal.* **2019**, *370*, 46–54.

[15] J. Lyu, X. Zhang, P. Li, X. Wang, C. T. Buru, P. Bai, X. Guo, O. K. Farha, *Chem. Mater.* **2019**, *31*, 4166–4172.

[16] a) T. Hansen, P. Vermeeren, R. Yoshisada, D. V. Filippov, G. A. van der Marel, J. D. C. Codée, T. A. Hamlin, *J. Org. Chem.* **2021**, *86*, 3565–3573; b) K. Doitomi, K. Xu, H. Hirao, *Dalton Trans.* **2017**, *46*, 3470–3481.

[17] a) T. Lu, F. Chen, *J. Comput. Chem.* **2012**, *33*, 580–592; b) T. Lu, Q. Chen, *J. Comput. Chem.* **2022**, *43*, 539–555.

Manuscript received: June 8, 2023
Accepted manuscript online: August 8, 2023
Version of record online: August 17, 2023